Keratin/Polylactic acid/graphene oxide composite nanofibers for drug delivery

(Article begins on next page)

19 July 2024

Keratin/Polylactic acid/graphene oxide composite nanofibers for drug delivery.

Gioacchino Schifino[1], Claudio Gasparini[1], Simone Drudi[2], Marta Giannelli[1], Giovanna Sotgiu[1,6], Tamara Posati[1], Roberto Zamboni[1,6] Emanuele Treossi[1], Emanuele Maccaferri[2], Loris Giorgini[2], Raffaello Mazzarro[3], Vittorio Morandi[3], Vincenzo Palermo[1], Monica Bertoldo [1,4,*] and Annalisa Aluigi[1,5,6*].

[1]Institute of Organic Synthesis and Photoreactivity – Italian National Research Council, Via P. Gobetti, 101, 40129, Bologna, Italy.

[2]Department of Industrial Chemistry "Toso Montanari", University of Bologna, Viale Risorgimento 4, 40126 Bologna, Italy.

[3] National Research Council, Institute for Microelectronics and Microsystems, Via Piero Gobetti 101, 40129, Bologna, Italy.

[4]Department of Chemical, Pharmaceutical and Agricultural Sciences, University of Ferrara, I-44121 Ferrara, Italy.

[5] Department of Biomolecular Sciences - School of Pharmacy, University of Urbino, Piazza del Rinascimento 6 - 61029 Urbino, Italy.

[6] Kerline srl, Via Piero Gobetti 101, 40129 Bologna, Italy.

[7] Department of Physics and Astronomy, Viale Berti Pichat 6/2, Università di Bologna, 40127 Bologna, Italy

ABSTRACT

In this work keratin/polylactic acid (PLA) 50/50 wt blend nanofibers with different loadings of graphene-oxide (GO) were prepared by electrospinning and tested as delivery systems of Rhodamine Blue (RhB), selected as a model of a drug. The effect of GO on the electrospinnability and drug release mechanism and kinetics was investigated. Rheological measurements carried out on the blend solutions revealed unsatisfactory compatibility between keratin and PLA under quiet conditions. Accordingly, poor interfacial adhesion between the two phases was observed by SEM analysis of a film prepared by solution casting. On the contrary, keratin chains seem to rearrange under the flux conditions of the electrospinning process thus promoting better interfacial interactions between the two polymers, thereby enhancing their miscibility, which resulted in homogeneous and defect-free nanofibers. The loading of GO into the keratin/PLA solution contributes to increasing its viscosity, its shear thinning behavior, and its conductivity. Accordingly, thinner and more homogeneous nanofibers resulted from solutions with a relatively high conductivity coupled with a pronounced shear thinning behavior.

FTIR and DSC analyses have underlined, that while the PLA/GO interfacial interactions significantly compete with the PLA/Keratin ones, there are no significant effects of GO on the structural organization of keratin in blend with the PLA. However, GO offers several advantages from the application point of view by slightly improving the mechanical properties of the electrospun mats and by slowing down the release of the model drug through the reduction of the matrix swelling.

1. INTRODUCTION

In the past few decades, electrospun polymer nanofibers have gained great interest as skin patches for drug delivery and wound management (Luraghi et al., 2021). Conventional wound dressings are made of woven and non-woven fibers of cotton, rayon, and polyesters (Dhivya et al., 2015). Significant advantages of electrospun patches are the nanostructured morphology resulting in high surface area and porosity that mimics the extracellular matrix (ECM).

Electrospinning is a widely used nanofabrication method to obtain nanofibers. It is easy to scale up and allows the processing of a wide variety of synthetic and natural polymers including blends. It allows also the easy encapsulation of drugs. Thanks to the high versatility, multicomponent electrospun layers with tunable chemical-physical properties can be properly designed and developed to target desired mechanical properties, drug release profiles, as well as biodegradability. Another advantage of electrospinning is the possibility to proceed through a layer-by-layer bottom-up approach and assemble different functional layers in a single, composite multilayer patch (Krysiak et al., 2021).

Owing to their structural and functional properties, as well as their biocompatibility, natural proteins are considered good candidates to prepare electrospun membranes for various biomedical applications (Akhmetova and Heinz, 2020). Among them, keratin is one of the most promising (Aluigi et al., 2015). It is an abundant protein, that can be found in the epithelial cells of mammals, birds and reptiles other than being the major component of feathers, wool, nails, and horns (Datta et al., 2020). Like collagen, the bioactivity of keratin proteins has been ascribed to the presence of specific amino acid sequences, such as arginine – glycine – aspartic acid (RGD) and leucine – aspartic acid – valine (LDV), that have a pivotal role in promoting cell adhesion and tissue regeneration (Verma et al., 2008). Due to its wide variety of amino acids,

keratin is an excellent carrier of hydrophilic, hydrophobic, and charged ingredients, thereby demonstrating great potential for the development of controlled drug delivery systems (Posati et al., 2018; Sadeghi et al., 2020). However, the processing by electrospinning of keratin proteins is rather challenging. Indeed, due to their low molecular weights (60-25 kDa for mammal keratins and 10 kDa for feather keratins), keratin solutions are generally characterized by excessively low viscosity, thereby resulting in unstable electrospraying, yielding droplets or beaded fibers. Blending with other polymers and/or reinforcing with fillers are strategies often used to overcome the aforementioned processing issues (Tonin et al., 2010).

Among the plethora of blending polymers proposed in the literature, polylactic acid (PLA) is considered attractive for biomedical applications due to its biocompatibility and good biodegradability (Li et al., 2009; Na Ayutthaya and Woothikanokkhan, 2013; Isarankura Na Ayutthaya et al., 2016). Furthermore, PLA is a polymer fully derived from renewable resources with a relatively high glass transition temperature (55–70 °C), low thermal conductivity, and high tensile strength (Saini et al., 2016). Depending on the stereoregularity degree, it can be semicrystalline or fully amorphous with corresponding different stiffness, elongation at break, as well as solubility properties. High stereoregular poly-L-lactic acid (PLLA) was found to allow electrospinning of keratin if added in an amount not lower than 50 % (Na Ayutthaya and Woothikanokkhan, 2013). The fibers produced with a mixture of organic solvents including formic acid, acetone, and chloroform exhibited a phase-separated core/shell morphology with the core of crystallized PLA (Isarankura Na Ayutthaya et al., 2016). The addition of clay nanoplatelet to the electrospinning solution was found to improve its processability and the capability of obtained nanofiber for removing methylene blue. (Isarankura Na Ayutthaya et al., 2016).

An alternative specific nanofiller not yet studied in a mixture with keratin is graphene oxide sheets (GO). It has been shown to improve the processing by electrospinning of many polymers and polymer blends (Gasparini et al., 2020; Ramazani and Karimi, 2015; Mao et al., 2018). In particular, Tan et al. observed that a small amount of GO contributes to increasing the solution viscosity (Tan et al., 2012). This thickener effect could improve the jet stability during electrospinning of low viscous solutions, such as the keratin-rich ones. Moreover, due to the large specific surface area and the abundance of functional groups, GO is known to display effective transport capacity of various drugs, and offers the opportunity to add stimulus controlled drug delivery ability to the systems (Mao et al., 2018; Zhou et al., 2014). For instance, GO incorporated in PLA nanofibers provided electrospun patches loaded with quercitin with electrically triggered release ability (Croitoru et al., 2021). Furthermore, according to the GO content, the electrical triggering capacity of the drug release could be tuned. Electrospun scaffolds of chitosan/poly(lactic acid)/GO/TiO2 loaded with doxorubicin (DOX) showed slower release of DOX in the presence of GO sheets as the effect of the pi-pi interactions between the carbon layers of GO and DOX (Samadi et al., 2018). Moreover, GO incorporated in chitosan/PLLA nanofibrous scaffolds was found to improve the antimicrobial activity of Gram-negative Escherichia coli (E. coli) and Gram-positive Staphylococcus aureus (S. aureus) as well as the proliferation of pig iliac endothelial cells and the ability to heal rats wounds (Yang et al., 2020).

In this study, to produce biodegradable and biocompatible material for controlled drug delivery, nanofibers mats of keratin/PLA/GO composites were fabricated via electrospinning. An amorphous PLA was selected since semicrystalline polymer's easiest phase-separated in blends for thermodynamic reasons (Jabarin et al., 2016). The miscibility degree of keratin and PLA,

under static conditions as well as under shear rate, was first studied by viscosity analysis of solutions under shear at different polymer blending ratios.

Focusing on a Ker/PLA 50/50 wt blend matrix, the effects of the interfacial interactions between GO sheets and polymer chains on the rheological behavior of the electrospun solutions, as well as on the nanofibers morphology, their thermal behavior, and their mechanical properties, were investigated. Finally, the role of GO sheets in the drug release mechanism from the composite electrospun mats was assessed using Rhodamine B, selected as a drug model because it is easy to detect and quantify.

2. EXPERIMENTAL

2.1 Materials. High molecular weight keratin (Ker) powder ($\approx$50 kDa) extracted from raw wool was kindly donated by Kerline Srl (Italy). Polylactic acid (PLA) pellet with an average molecular weight (Mn) of 119 000 Da and a polydispersity index (Mw/Mn) of 1.40 was kindly provided by Nature Works LLC (Ingeo 4060D). 1,1,1,3,3,3-Hexafluoro-2-propanol (HFIP) was purchased from Sigma Aldrich S.r.l. Graphene Oxide (GO) solutions with sheets having a thickness of 1.1 $\pm$ 0.2 nm and lateral sizes of 120 $\pm$ 30 nm were prepared through a modified Hummers method (Gasparini et al., 2020).

2.2 Preparation of keratin/PLA blend solutions at different blending ratios. Keratin and PLA pellets were separately dissolved in HFIP at a concentration of 10 % w/v by stirring for 4 hours. Ker/PLA blends at weight ratios 0/100, 25/75, 50/50, 75/25, and 100/0 between the two polymers were obtained by mixing the desired volumes of the pure keratin and PLA solutions prepared before. Mixtures were homogenized by stirring overnight at room temperature.

2.3 Preparation of keratin/PLA blend film. Ker/PLA 50/50 blend films were prepared by casting the relative blend solution and letting it dry for 24 hours at room temperature in a chemical hood.

2.4 Preparation of Ker/PLA composite nanofibers loaded with different amounts of graphene oxide. For the preparation of Ker/PLA 50/50 nanofibers, the keratin and PLA pellets were separately dissolved in 4 mL of HFIP at a polymer concentration of 10 % wt. under shaking for 2 hours. The solutions were mixed and stirred at room temperature for 24 h. GO doped Ker/PLA 50/50 composite solutions were prepared by dispersing the desired amount of GO into HFIP under vigorous sonication in an ultrasonic bath (Elmasonic S 30 H, 37 kHz) for 1 h. Composite solutions containing 0.1, 0.5, 0.7 1 % wt. of GO concerning the weight of the total polymer (Ker + PLA), were prepared as described before but using properly GO doped HFIP as solvent. For nanofiber preparation, the blend solutions were loaded into a 5 mL plastic syringe connected to a needle having an inner diameter of 0.603 mm. The syringe was placed horizontally on the syringe pump (KdScientific) and a voltage supply (ALINTEL SHV 150, 5 mA, ±30 kV) was attached to the needle tip; while a metal collector plate was grounded. The polymer solutions flow rate was 1.8 mL/h. The distance between the needle tip and the static collector was set to 12, 15, and 18 cm; the used applied voltage was 12, 15, and 18 kV. Electrospinning was conducted under controlled conditions of temperature (24.0 ± 0.5 °C) and relative humidity (20−40 %).

2.5 Characterizations. Shear rate-dependent viscosity measurements of the polymer blends and polymer blend/GO nanocomposites loaded with different amounts of GO were determined in HFIP solution with Anton Paar Compact Rheometer MCR 102 equipped with a PDT 200/56/l Peltier temperature control device. Analyses were carried out at 25 (±0.1) °C by using a parallel

plate geometry in a controlled shear rate mode. The gap opening was 0.45 mm. Shear rate was varied in the 0.1 to 1000 s^{-1} range using a logarithmic ramp; while the respective acquisition time was logarithmically decreased from 10 s to 1 s. Data were acquired and elaborated with the RheoCompass Software (Anton Paar GmbH). For each sample, the final viscosity vs shear rate curve is the average of 4 analyses.

The morphology of cryogenic sections of the blend film, as well as the electrospun blend nanofibers, were investigated by scanning electron microscope (SEM) using a Zeiss EVO LS 10 instrument equipped with a LaB6 source. The film was frozen by immersion in liquid nitrogen for 2 minutes and then fractured (with the help of two tweezers) to obtain the cryogenic section for observation. All samples were gold-sputtered for 1 min before the analysis. The acceleration voltage was 5 kV and the working distances were 4.3 mm or 5.2 mm.

The nanofiber diameters were obtained by using ImageJ software (National Institutes of Health, Bethesda, MD). In particular, the mean diameter and the diameter distribution of nanofibers were obtained from 150 measurements randomly gathered from different SEM images of the same sample. The distribution of GO in the electrospun nanofibers was examined by an FEI Tecnai F20 High-Resolution Transmission Electron Microscope (HR-TEM), equipped with a Schottky emitter operating at 120 kV. A thin layer of composite fibers was electro-spun directly on a Quantifoil R2/1 Carbon film-coated copper TEM grid.

Tensile tests of electrospun mats were made using a Remet TC10 universal testing machine equipped with a 10 N load cell at a crosshead separation speed of 10 mm/min. The nanofibrous mat was anchored to a paper frame to prevent membrane damaging and slipping from the machine supports. Specimens had a dimension of 20 × 30 mm, width, and gage length, respectively.

Raw load-displacement data were treated to obtain stress-strain data. The strain (ε) was calculated by dividing the displacement (δ) by the initial specimen length (gage length, L) as follows:

$$\varepsilon = \frac{\delta}{L}$$

The stress (σ) calculation was done by applying the following formula (Maccaferri et al., 2022; Maccaferri et al., 2020; Maccaferri et al., 2021):

$$\sigma = \rho_m \frac{F}{m} L$$

where ρ_m is the material density (mg/mm^3), F is the load (N), m is the specimen mass (mg) and L is the specimen initial length (mm); σ is expressed in MPa.

The mats' elastic modulus and properties at break (maximum stress, σ_{max}, and strain at break, ε_{max}) were determined from σ-ε curves. The elastic modulus was evaluated via linear regression of stress-strain data in the 0–1% deformation range. σ_{max} and ε_{max} are the highest values of stress and strain, respectively, at which the membrane break occurs.

Infrared spectra of nanofiber mats and films were acquired with a Bruker Vertex 70 interferometer equipped with a diamond crystal single reflection Platinum ATR accessory, in the 4000–600 cm^{-1} region, with 100 scans and a resolution of 4 cm^{-1}.

Differential scanning calorimetry (DSC) was performed with a PerkinElmer DSC 8000 equipped with an intercooler II cooling device and Software Pyris for data acquisition and analysis. Analyses were accomplished under a nitrogen atmosphere (30 ml/min) on 5-8 mg of sample in an open aluminum pan. Program temperature was: heating from 20 to 105°C, cooling back to 20°C, and heating to 170 - 200°C (second scan) at 10°C/min as scanning rate. Data

analysis was performed on the second scan step. The instrument was calibrated with Indium and lead as standards.

Thermogravimetric analysis (TGA) was performed with Perlin Elmer TGA4000 equipped with software Pyris for data acquisition and analysis. 6-7 mg of sample in alumina pan analyzed in the 25-900 °C temperature range under nitrogen atmosphere (50 ml/min) at 10°C/min as heating rate.

2.6 Drug Release. The electrospun mats loaded with 3 % wt. of rhodamine B (RhB) were specially prepared for the drug release test. The samples were prepared as described before, simply adding the desired amount of RhB in the polymer solutions before electrospinning.

To determine the drug release profiles, 1 square piece (2cm x 2cm) of the electrospun mat was placed inside dialysis bags with a cut-off of 12-14 kDa and put in 6mL of phosphate buffer at pH 7.4. The release tests were carried out at a temperature of 37 °C. Aliquots of 100 μL were withdrawn at specific time intervals and replaced with fresh buffer; the released RhB was detected as intensity in the UV-Vis spectrum at 554 nm, after the determination of a calibration curve (shown in Figure S1 of the supporting information). Spectra were collected by using a UV-Vis a Cary 100 - Agilent Technologies spectrophotometer. Reference tests with RhB were carried out with an aqueous solution of RhB at 3 % wt. (500μL) in the dialysis bag.

3. RESULTS AND DISCUSSION

3.1 Miscibility of keratin and PLA in HFIP solutions. The miscibility degree of keratin and amorphous PLA dissolved in HFIP at different blending ratios and a total polymer concentration of 10 % wt was evaluated by viscosity analysis under continuous shear (Figure 1). HFIP was selected being the only solvent capable of dissolving both keratin and PLA. It is also an excellent

solvent for electrospinning due to its relatively low surface tension and sufficiently high dielectric constant (Eren Boncu et al., 2020). It is commonly used to develop electrospun mats for biomedical applications and the non-toxicity of the obtained nanofibers has been demonstrated in several scientific papers (Ulker Turan and Guvenilir, 2021; Eren Boncu et al., 2020; Guidotti et al., 2021).

Bare Keratin at a low shear rate showed an almost yield-stress liquid behavior (Otsuki, 2020) with a very small reminiscence of a Newtonian plateau below shear rate 0.3 s^{-1}. Yield-stress-like plots at low shear rates are typically observed on water solutions of globular proteins (Castellanos et al., 2014). The behavior has been attributed to adsorption at the interface and aggregation phenomena (Sharma et al., 2011). The latter effect has been reported to be the dominant one when surfactants are present (Castellanos et al., 2014). Although the adsorption of keratin at the plate interface during analysis could be the dominant effect casing the yield-stress-like behavior in pure keratin, the effect seems to be less important when Keratin is blended with PLA. In fact, all viscosity plots of Keratin/PLA mixtures seem to exhibit a Newtonian-like plateau at a low shear rate (Figure 1). The difference with pure keratin suggests that in the blend, the continuous phase is mainly made of PLA and keratin is in separated dispersed domains. Indeed, pure PLA shows the typical behavior of neutral polymer solutions, with the Newtonian plateau at a low shear rate. By a more careful analysis (Figure 1) the viscosity at the lowest investigated shear rate is not constant and it decreases slowly with the shear rate. This suggests a reminiscence in the blend also of the adsorption/desegregation phenomena for keratin hypothesized in the pure keratin solution. Then, in the blend plots, a more or less defined plateau can be identified. This particular plot shape can be due to the superposition of the pure PLA plateau and the decreasing viscosity of keratin because of the adsorption/desegregation

phenomena, even if this last seems reduced by the intensity in the blend. This behavior supports the hypothesis of the presence of keratin in separated dispersed domains, at least at a low shear rate. After this initial part of the plot, named region I at least others two regions are noticed, named II and III in Figure 1.
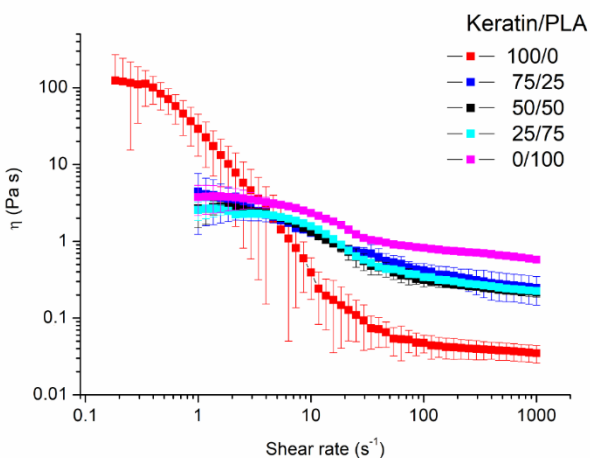
Figure 1. *Viscosity under continuous shear (η) of the Keratin/PLA blend solutions at different blending ratios.*

Region I is up to a shear rate of 4-5 s^{-1}, the second one up to 11-12 s^{-1}, and the third up to 1000 s^{-1}. The second region is characterized by the pronounced viscosity decrease with the shear rate typical of polymer solutions, which is due to chain elongation under flux. At this shear rate, PLA chains align. The behavior is observed even in keratin after the small step of the region suggesting the occurrence of disaggregation or changes in the chain conformation of the protein also. The rearrangement would promote the transition from an almost insoluble globular structure of the protein to a more soluble and less compact one. A similar effect has been reported also for chitosan at 70 °C (Pakravan et al., 2012). Chitosan shares with keratin some important structural features such as the presence of ionizable groups and the ability to form intra- and inter-chain hydrogen bonds. This effect in chitosan was reported already at a lower

shear rate. However, it cannot be excluded that this occurred in keratin also, in particular in blends. Finally, in the third region, the slope of the viscosity plot decreases, and a new plateau seems to be approached indicating that the entanglements between chains and/or stable intra-chain hydrogens bonds prevent additional chain elongation. The viscosity observed at this shear rate is one of the stretched networks.

Despite the different phenomena responsible for the observed viscosity at a very low shear rate, the values were used to extract information on the expected behavior in the quiet conditions of the film casting process. Furthermore, the values at 100 s^{-1} shear were assumed to represent the condition during electrospinning (Beliciu and Moraru, 2011). In fact, this shear rate is usually associated with several shear processing operations such as pumping and extrusion by spinning, including electrospinning (Beliciu and Moraru, 2011). For the miscibility analysis, the experimental values obtained at the aforementioned shear rate values were compared with the ones calculated by applying the additive mixing rule for ideal mixtures (equation 1):

$$ln\ \eta_T = \sum_i w_i\ ln\ \eta_i \qquad\qquad\qquad (1)$$

where ω_i and η_i are the weight fraction and the viscosity of the ith component, respectively and η_T is the total viscosity of the blend (Teodorescu et al., 2018).

In quiet conditions, the observed values of viscosities were lower than the additively predicted ones at all investigated compositions, resulting in a concave plot of η_T as a function of the composition (Figure 2a). Negative deviations are usually associated with the occurrence of slip, caused by a lack of adhesion (weak interactions) between the two polymers (García-Abuín et al.,

2010). Notice that, even though the calculated value at a low shear rate would suffer from a possible overestimation of the viscosity of pure keratin, the experimental values for the blends do not follow a linear plot, rather they follow a convex curve, thus suggesting the absence of compatibility between the two components. The result is in agreement with a biphasic morphology in which PLA is the continuous phase and keratin is the dispersed one. In such a case, the blend behavior would be similar to the one of the continuous phase with the Newtonian plateau of PLA.

Accordingly, as is typically the case of weakly interacting polymers, the morphology of the solid Ker/PLA 50/50 blend showed separate phase domains by SEM analysis of the cryogenic section. Furthermore, detachment at the interface was detected. The presence of interstices between the phases (indicated by the red arrows in Figure 2b) indicates poor interfacial adhesion and unsatisfactory compatibility between the two polymers. On the contrary, at the higher shear rate of 100 s^{-1}, the experimental viscosities were higher than the one predicted by the additive rule (Figure 2c), thereby suggesting good adhesion between the blend components.

Most likely, the keratin conformation under flux enables a more effective interaction with the PLA chains through hydrophilic and/or hydrophobic interactions. Accordingly, homogeneous nanofibers were obtained by electrospinning the ternary mixture (Figure 2d).

The HFIP is highly volatile (Boiling point 58°C), and thus evaporates rapidly during electrospinning fixing the structure assumed by the spun material.
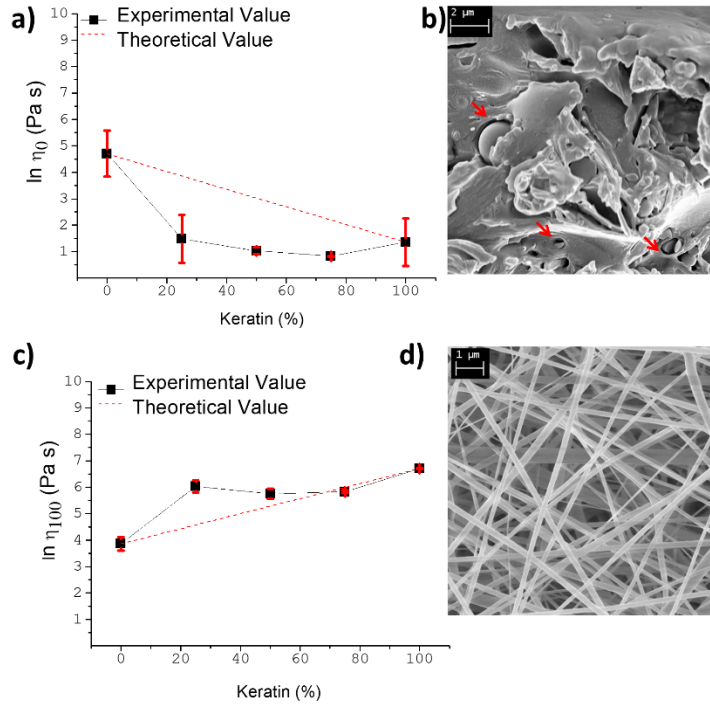
**Figure 2**. *a)* $\ln \eta_0$ *(evaluated at 100 s^{-1}) as a function of keratin content: comparison between*

experimental values (—■—) and theoretically estimated from the rule of ideal mixtures shown in eq. 1 in the main text (----); b) cryogenic section of the cast film obtained from the keratin/PLA 50/50 blend solution, observed at the scanning electron microscope; c) $\ln \eta_{100}$ *as a function of*

keratin content: comparison between experimental values (—■—) and theoretical values (----) estimated from the rule of ideal mixtures shown in eq. 1 in the main text; d) electrospun membrane (obtained at 18 kV, 1.8 mL/h, 15 cm) observed at the scanning electron microscope.

Accordingly, when a less volatile solvent made of a mixture of chloroform/acetone with formic acid was used, fiber with a core/shell morphology was instead obtained(Isarankura Na Ayutthaya et al., 2016). On the contrary, by using HFIP, fibers were very smooth thus suggesting not only compatibility but also miscibility between the two polymers. Miscibility induced by flow has been often reported and theoretically described (Horst and Wolf, 1997; Jupp et al., 2003; Chopra et al., 1999). Notice that, the use of an amorphous PLA, instead of a crystallizable one

(Isarankura Na Ayutthaya et al., 2016), would have contributed to avoiding phase separation during the fiber formation.

3.2 Effect of GO on the Keratin/PLA blend solutions. For the sake of brevity, the Ker/PLA 50/50 mixture was chosen as the matrix to study the effect of doping with GO sheets. At first, the viscosities of GO dispersions in the Ker/PLA 50/50 blend solutions were analyzed. Figure 3 shows the apparent viscosities versus the shear rate of the Ker/PLA 50/50 blend with different amounts of GO sheets, on a log-log scale. The shear rate regions I, II, and II, individuated for the blends without GO are indicated also in the graph.
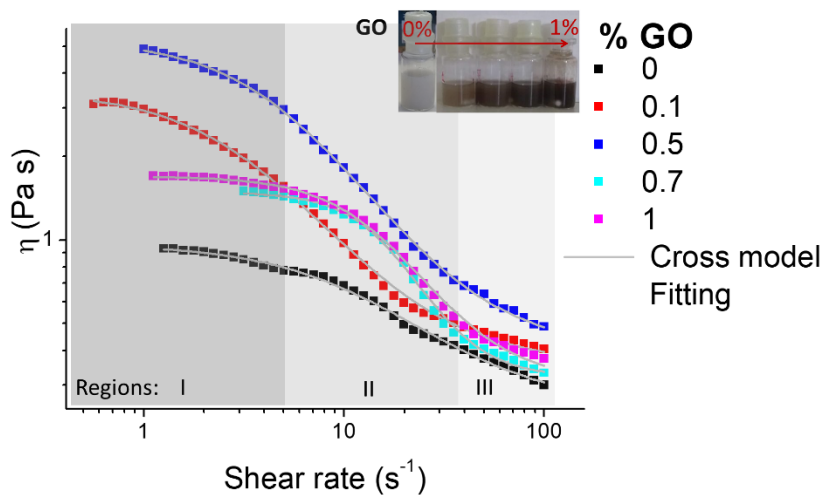
Figure 3. *A visual image of the keratin/PLA solutions containing different amounts of GO sheets and related viscosities vs shear rate.*

All curves included one of the net polymeric matrices, show the apparent viscosity, and decrease with the shear rates more or less in all the three regions. Distinct effects of GO loading in the three above indicated regions of the viscosity plots were noticed: in the first region, a viscosity increase depending on the GO content was observed at 0.1 or 0.5 % loading. At these loadings,

the viscosity depends on the shear rate much more than it occurs in the net matrix with a dependence similar to the one of the bare keratin (Figure 1). On the contrary, for higher GO amount (0.7 or 1 %) the viscosity plots have a shape comparable to the one of the blend matrix even though the viscosity is higher. However, the increase does not seem to depend on the loading, since the flow curves at 0.7 and 1 % of GO are almost superimposed on each other. The viscosity of bare GO in HFIP is negligible in all the investigated range of shear rate and at all investigated concentrations (Figure S2). Therefore, no one of the observed features of the viscosity plots of Ker/PLA/GO can be ascribed to a simple additive effect of the mixture components. The presence of interactions between GO and the polymeric matrix is then clearly indicated. The extent and/or the consequence of this interaction depends on the GO amount. The effect higher at low GO loading suggests the presence of an additional effect. In particular, it seems that in the presence of a low GO amount, keratin recovers the behavior it has in the absence of PLA. Therefore, the high viscosity can be explained under the hypothesis used to explain the first part of the bare keratin plot, that is, the proteins adsorb at the plate interface of the rheometer or rearranges under flux. Most likely at this composition, an inverted or co-continuous phase domain morphology build-up with keratin not only segregated in dispersed domains as it does in the absence of GO. GO promotes both viscosity and yield-stress increase. When the amount of GO is 0.7 or 1 % the viscosity plots are similar to the one of the pure blend matrix but with a higher initial viscosity thus suggesting that the PLA/GO phase is the continuous one as in the blend matrix, and GO causes the viscosity increase. By a careful comparison of the initial plateau, a small difference between the viscosities at the two loadings level, namely 0.7 and 1 % can be noticed. The difference seems negligible because much smaller than the one observed for lower GO loading, but it is not much smaller than other reported

differences in the literature (Choi et al., 2001; Hyun et al., 2001). An effect of GO loading on the viscosity values is present in the second and third regions as well, while a negligible effect on the yield-stress seems to result from an increase of the GO from 0.7% to 1%. Based on this data, it seems that at least in solution two different classes of nanocomposites are obtained. The first for GO loadings up to 0.5 %, where two co-continuous keratin and PLA/GO rich phases form, and a second for loading > 0.5 %, where PLA/GO is the continuous phase.

To have a better understanding of the effect of the GO loading, the viscosity curves were analyzed through the Cross model (eq. 2). The model is commonly used to describe the low-shear-rate viscosity, η_0 (Pa s), of shear-thinning fluid(Hauswirth et al., 2020):

$$\frac{\eta - \eta_\infty}{\eta_0 - \eta_\infty} = \frac{1}{1 + (\lambda \cdot \dot{\gamma})^n} \tag{2}$$

In the equation, η_0 (Pa s) is the apparent viscosity at any shear rate $\dot{\gamma}$ (s^{-1}) and η_∞ (Pa s) is the viscosity at the very high shear rate, λ (s) is the time constant correlated to the relaxation time of polymer chains and n is a dimensionless rate constant, known as the (Cross) Rate Constant, indicating the degree of dependence of viscosity on the shear rate in the shear-thinning region.

A value of 0 for n indicates Newtonian behavior, while n values tending to unit indicate shear-thinning behavior. The best fitting of the experimental data with the Cross model gives $R^2 >$ 0.90. Even if the accordance was not perfect, as expected by the quite complex shape of the plots, the calculated parameters (Table 1) were assumed reliable, at least for comparative purposes. The obtained zero shear rate viscosities η_0 were found to increase with increasing the GO concentration from 0.1 to 0.5 %, whereas a further GO increase from 0.7 to 1 % reduces both

viscosities. This behavior numerically describes the effect of the GO loading on promoting a different phase organization. Accordingly, the initial η_0 increases up to GO 0.5 % because of the increasing thickening effect induced by GO sheets.

Cross-model values of n approaching 1 were obtained for all the investigated solutions, thus confirming the presence of a continuous or co-continuous phase made of keratin, which typically gave strong shear thinning behavior. Moreover, samples containing 0.1 and 0.5 % of GO showed the highest values for λ among the investigated compositions, suggesting a slower relaxation dynamic due to the protein components interacting with GO. On the other hand, at higher GO loading the rheological behavior is dominated by the PLA phase, and a less effective shear thinning behavior is observed (or pseudoplastic behavior). In other words, GO is less effective in reducing the rate of PLA than keratin relaxation.

Table 1. *Cross model parameters related to Keratin/PLA 50/50 solutions doped with different amounts of GO sheets.*

% GO	η_0 (Pa s)	η_∞ (Pa s)	λ (s)	n	R^2
0	1.00±0.02	0.12±0.02	0.074±0.004	1.00±0.08	0.996
0.1	3.9±0.1	0.23±0.04	0.36±0.03	0.99±0.06	0.996
0.5	6.1±0.3	0.13±0.08	0.24±0.02	0.99±0.07	0.996
0.7	1.9±0.1	0.3±0.1	0.10±0.02	0.9±0.1	0.948
1	1.7±0.1	0.31±0.01	0.065±0.001	1.0±0.2	0.911

3.3 Nanofibers Morphology. Figure 4 shows the scanning electron microscope (SEM) images of the keratin/PLA 50/50 nanofibers, as well as of their nanocomposites obtained with different GO loadings and different applied voltages. The relative diameters distribution curves fitted with the LogNormal function are shown in Figure S3. As shown, the electrospinning of Ker/PLA 50/50 solution, as well as of all the relative GO composite suspensions, gives rise to smooth and defects-free nanofibers with random orientation, having a mean diameter between 270 and 120

nm. In Figure 5, the mean diameters as a function of GO loading and applied voltage are reported. Unfortunately, the complexity of the electrospinning process makes often the determination of the operational parameter effects on nanofibers morphology very difficult if not impractical. In general, the higher viscosity of the polymer fluid generates a higher opposing force to the jet stretching and thinning, thus leading to greater nanofibers. On the other hand, more conductive solutions allow a greater stretching of the electrospinning jet, due to the presence of more charge carriers, thus favoring a reduction of the fiber diameter.

As can be seen, for the GO doped solutions, higher applied voltages produced thinner nanofibers and this could be attributed to the increasing stretching force with increasing the intensity of the electrostatic field (Haider et al., 2018). Instead, at lower voltages of 12 and 15 kV, a decrease of the mean diameters of the fibers with increasing the GO loading until 0.7 % occurs, notwithstanding the higher viscosities of GO doped solutions compared to the solution without GO. Probably, for these electrospinning conditions the enhanced jet thinning with increasing the GO amount is due to the conductivity increase of the GO doped solutions with increasing the GO amount (Figure S4) (Heikkila and Harlin, 2009; Xiao et al., 2016; Liu et al., 2017).

The most pronounced shear-thinning behavior of the GO doped solutions could also contribute to producing thinner nanofibers by promoting the macromolecular orientation along the drawing direction induced by the electric field. Nevertheless, the slight increase in the mean diameters, observed for the fibers containing 1 % of GO, notwithstanding the highest conductivity of the related solution (Figure S4), could be attributed to the less pronounced shear thinning of the solution doped with 1 % of GO concerning the other ones.

At the highest applied voltage, namely 18 kV, the deposition rate seems to be too much faster to allow chain elongation, and the dominant effect is the one of viscosity as was reported for PLA/keratin/clay electrospun at 19 kV(Isarankura Na Ayutthaya et al., 2016).

The distribution of the GO sheets on the nanofibers was investigated by HR-TEM analysis (Figure 6). As previously observed by SEM, the thickness of the nanofibers is quite polydispersed, ranging from > 600 nm to less than 100nm. The addition of GO in the nanofibers resulted in the formation of bulges protruding from the fibers. The bulges displayed different sizes, often exceeding the thickness of the fiber. We should note that the diameter of nanofibers (spanning from 87 nm up to 261 nm in the different samples) is comparable to or lower than the average size of the GO sheets (120 ± 30 nm). High magnification micrographs of the bulging region (Figure 6c) displayed diffraction fringes of a semi-crystalline material with an average d-spacing equal to 0.40 nm, compatible with GO (002) lattice planes, often observed on GO nanosheets wrinkles and folded edges (Li et al., 2021). The presence of GO in the bulging region was further confirmed by electron diffraction images (Figure S5). We cannot exclude the presence of GO fully embedded in the nanofiber structure along the main axis, but the limited contrast due to the material's likeliness and the lack of distinct diffraction patterns does not allow for a full understanding of the nanofibers' internal structure.
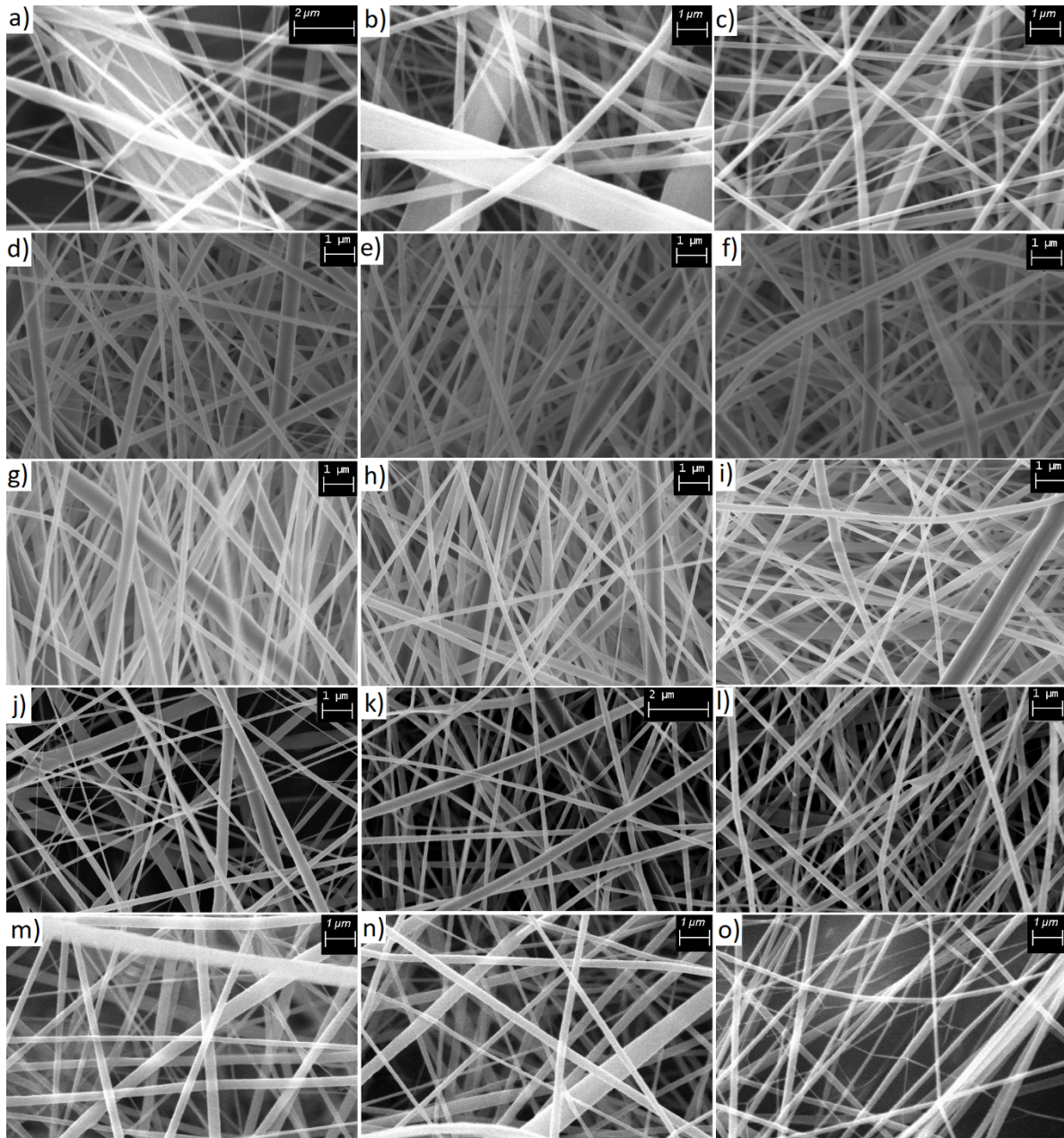
Figure 4. *SEM images of electrospun fibers from keratin/PLA 50/50 solutions with different loadings of GO sheets obtained using a flow rate of 1.8 mL/h and a tip-to-target distance of 15 cm: a) 12 kV – 0 % GO; b) 15 kV – 0 % GO; c) 18 kV – 0 % GO; d) 12 kV – 0.1 % GO; e) 15 kV – 0.1 % GO; f) 18 kV – 0.1 % GO; g) 12 kV – 0.5 % GO; h) 15 kV – 0.5 % GO; i) 18 kV – 0.5 % GO; j) 12 kV – 0.7 % GO; k) 15 kV – 0.7 % GO; l) 18 kV – 0.7 % GO; m) 12 kV – 1 % GO; n) 15 kV – 0.7 % GO and o) 18 kV – 1 % GO.*
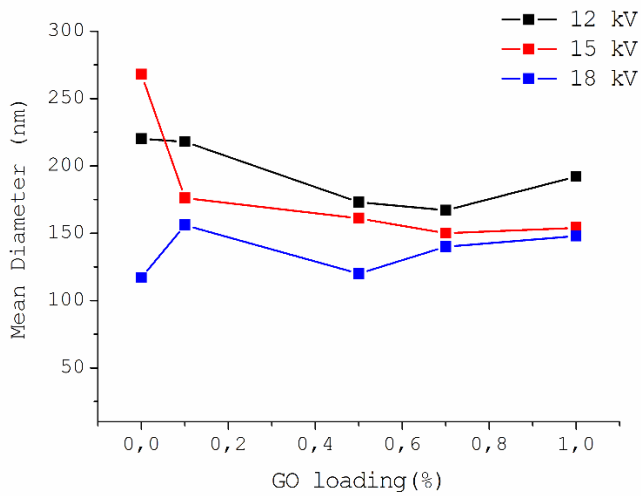
Figure 5. *Fibers mean diameter at different GO loading and different applied voltages*
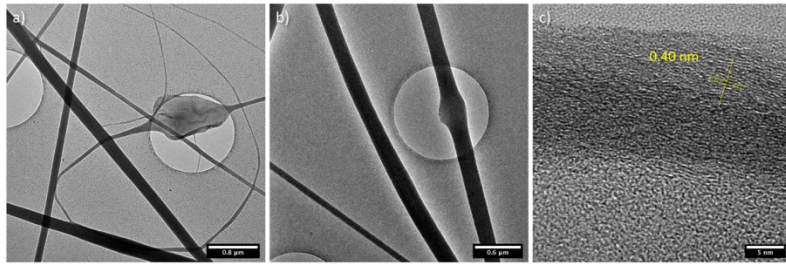
Figure 6. *TEM images of keratin/PLA 50/50 with a) 0.5 % of GO and b) 1 % of GO; c) detail at higher magnification of the keratin/PLA 50/50 with 0.5 % of GO.*

Among all the considered electrospinning conditions, a voltage of 18kV, a working distance of 15 cm, a flow rate of 1.8 mL/min, and a deposition time of 2 hours was selected as the best parameter to obtain mats with more homogenous nanofibers showing narrower diameter distributions (**Figure S2**) at all the GO loadings.
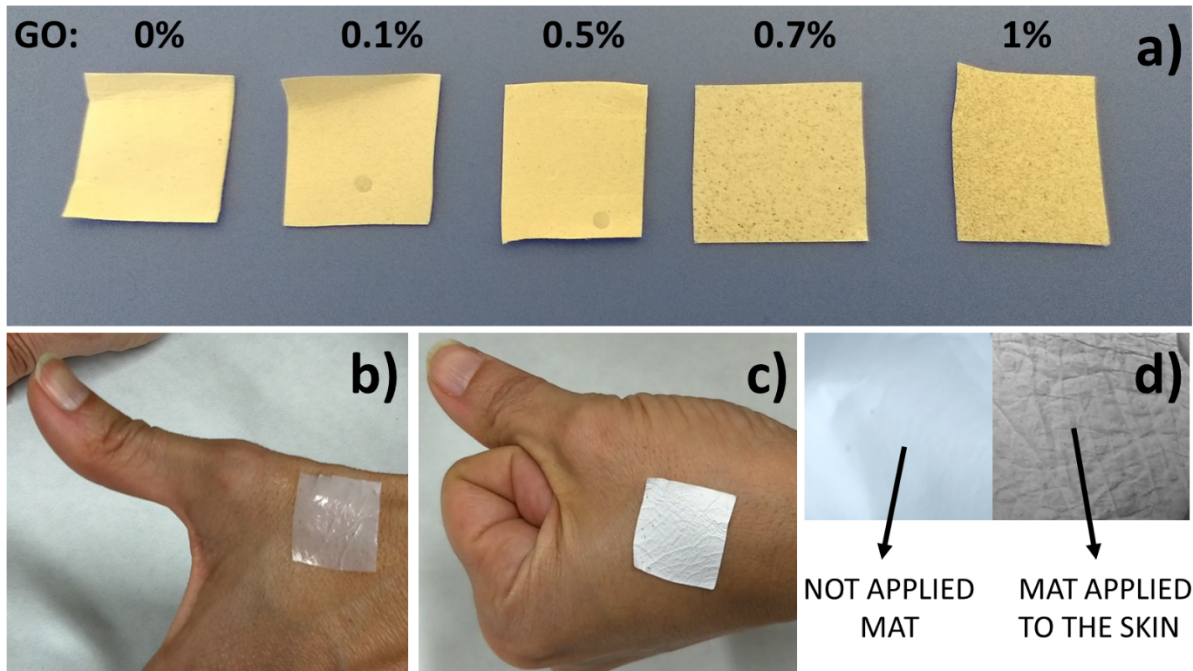
Figure 7. a) square pieces of keratin/PLA/GO electrospun mats at different loadings of GO; b) electrospun mats on the wet skin; c) after drying and d) conformal contact of the electrospun mat evidenced by the comparison between the not applied mat and the mat applied to the skin.

In Figure 7a, square pieces of Ker/PLA/GO electrospun mats at different loadings of GO are shown. The mats can be easily handled (see video support), they exhibit robust adhesion on wet skin (Figure 7b) that is maintained even in the dry skin (Figure 7c) since they can achieve conformal contact replicating human skins pattern (Figure 7d). This behavior could be explained by assuming a muco-adhesion process, typical of several proteins. In muco-adhesion, there is an intimate contact between the adhesive material and the skin, caused by wetting and swelling of the material followed by the formation of chemical bonds (such as hydrogen bonds) and/or Van der Waals forces.

3.4 Interaction studies between Keratin, PLA polymer chains and GO. Figure 8a shows the characteristics of ATR-FTIR adsorption peaks, in the 2000-800 cm^{-1} range, of keratin (red line),

PLA (blue line) regenerated from HFIP by electrospinning, and GO (black line) regenerated from HFIP by solvent casting. In particular, keratin adsorption peaks fall at 1650 cm^{-1} (Amide I), 1532 cm^{-1} (Amide II), 1213 cm^{-1} (Amide III), and 1190 cm^{-1} and 1021 cm^{-1} (asymmetric and symmetric cysteine-S-sulphonated groups, respectively). Instead, the PLA shows a strong adsorption band at 1749 cm^{-1} due to the carbonyl stretching vibration, at 1180 cm^{-1} and 1080 cm^{-1}, due to the C-O-C asymmetric and symmetric stretching, respectively. The peak at 1452 cm^{-1} and 1360 cm^{-1} are due to CH$_3$ asymmetric stretching and CH$_3$ groups bending, respectively(Zhang et al., 2004). According to the literature data, the GO sheets showed the characteristic adsorption peak at 1722 cm^{-1}, due to the C=O stretching, 1613 cm^{-1} related to the non-oxidized skeletal component of graphite, 1049 cm^{-1} and 984 cm^{-1} attributed to the C-O and C-C stretching vibrations, respectively (Rostami et al., 2020).

In the 1700-1820 cm^{-1} spectral region, where there are no adsorptions of keratin (Figure 8b), we can observe the carbonyl stretching peak associated with the PLA (at 1746 cm^{-1}), shifted towards higher wavenumbers when blended with keratin (1752 cm^{-1}).
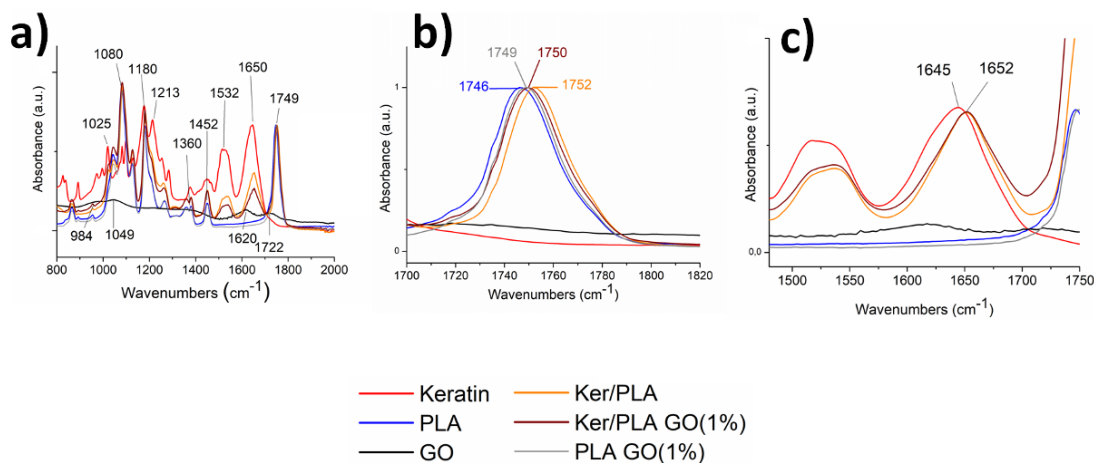
***Figure* 8.** *a) ATR-FTIR spectra of keratin powder (red line), PLA nanofibers (blue line), GO (black line), keratin/PLA 50/50 nanofibers (orange line), and keratin/PLA 50/50 nanofibers containing 1 % of GO (wine line), PLA nanofibers containing 1 % of GO; b) spectra in the 1746-*

The 6 cm^{-1} shift of the whole peak is in agreement with the formation of a miscible blend of the two components in the nanofibers. The shift toward higher wavenumbers, differently from the red shift more commonly observed in these systems, indicates a less restrained arrangement of the PLA chains in the mixture so that the steric hindrance of the PLA carbonyl groups is reduced and their vibration energy is increased. A slight shift towards higher wavenumbers was observed also for the PLA nanofibers containing the 1 % of GO sheets (from 1746 cm^{-1} to 1749 cm^{-1}). This data suggests that in the presence of the GO sheets, the PLA chains assume an organization similar to the one assumed in the presence of keratin. Moreover, the C=O adsorption peak of the keratin/PLA/GO ternary system seems the result of the PLA/GO and PLA/Keratin interfacial interactions since it falls at 1750 cm^{-1} and it is broader towards higher wavenumbers. This data supports the formation of almost homogenous mixtures of the three components even in the solid state, at least with 1 % GO in Ker/PLA 50/50. In fact, under this circumstance, the number of PLA/Ker interactions would be reduced by the competition with the PLA/GO ones, thereby producing a lower C=O shift. The whole result would be the observed intermediate shift. On the other hand, by analyzing the amides spectra region of keratin (1480-1750 cm^{-1}) where there are no adsorptions of PLA, a shift towards higher wavenumbers of the Amide I in the keratin/PLA sample (with no GO) with respect to the keratin was also observed (Figure 8c). This blue shift suggests that changes in the secondary structures of keratin occur under the electrospinning most likely resulting in more elongated configuration chains. Similar results have been reported for PLA/keratin/clay nanofibers, where the nanoclay was found to increase the fraction of keratin in α conformation (Isarankura Na Ayutthaya et al., 2016), a structure that may form more easily in

elongated chains than β-one does. No significant differences were observed in the Amides I and II with the introduction of GO, thereby supporting the hypothesis of negligible effects of the GO in the polymer matrix rearrangements when loaded in a large amount.

3.5 Thermal behavior. The effect of different GO loadings on the thermal stability of keratin/PLA electrospun mats was studied by TGA in a nitrogen atmosphere. The recorded data indicates good thermal stability with a weight loss of 5 % at around 225 °C at all investigated compositions (Figure 9). In fact, the addition of the thermostable PLA to keratin improves the thermal stability of the protein (Figure S6). On the contrary, the presence of GO at different percentages of loading was found to have a negligible effect on the thermal stability of the matrix and the degradation pathway. In fact, the thermograms for the composites with different GO content are almost all superimposed with only minor differences in the 400-900 °C thermal region. The differences are in the range of instrumental error and thus no correlation with the GO content was found. A similar effect has been observed also for GO in the pure PLA (Figure S6). This behavior is different from the ones described in the literature for GO dispersed in other polymeric matrices, such as polypropylene (Sabet et al., 2020), nylon 6 (Xiao et al., 2016), and poly(ethylene-co-vinyl alcohol) (Yassin and Abdelghany, 2021) where a significant increase of thermal stability was observed, with the effect depending on the GO loading. However, apparent contradictory results are also reported for GO in PLA and keratin, for which either a decrease in the thermal stability or an increase has been reported (Liu et al., 2017; Zhang et al., 2020; Wu et al., 2020; Esparza et al., 2017). The differences between the different data in the literature can be interpreted as differences due to the functionalization of GO (in the case of PLA) and to the matrix feature, such as the presence of poly(ethylene oxide) as a blend component (in the case of keratin), as well as differences in the interaction between GO and the polymeric matrix. In order

to verify the possible different effects of GO on the two components of our matrix (namely PLA and keratin), GO was incorporated into PLA with a GO loading of 0.5 %. The TGA of this sample (Figure S5), showed no significant shift toward either higher or lower temperatures than the one of the matrix for the composite, thus indicating the absence of any effect of GO both on the thermal stability of PLA and on that of the Ker/PLA 50/50 blend.
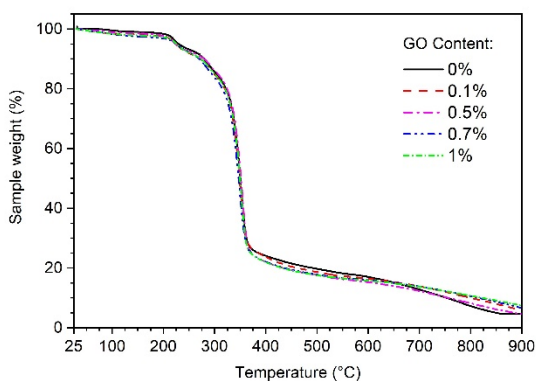
Figure 9. Comparison among the TGA plots of Ker/PLA blends with different loadings of GO.

The thermal behavior of the Ker/PLA 50/50 blend in the presence of the different amounts of GO was studied also by DSC analysis. After the first heating step up to 105 °C to remove the possible adsorbed moisture and solvent residual from electrospinning, samples were analyzed from room temperature up to 200 °C, namely in the range of thermal stability of the composites by TGA analysis (Figure 10a). In this range, a well detectable glass transition process was observed in all samples between 55 and 56 °C (Table 2). The value can be assigned to the PLA phase into the immiscible Ker/PLA blend. Indeed, the modest 3 °C shift toward higher temperature with respect to pure PLA indicates immiscibility between the two polymers in the blends. This result is further supported by the perfect proportion between the ΔCp in the blend and in the pure PLA, which indicates that all PLA participate in the separated phase. On the

other hand, the small shift toward the high temperature of the glass transition of PLA in the blend with respect to the pure polymer can be due to any chemical interaction at the interface with keratin by hydrogen bonding or dispersive force. These interactions can result in reduced mobility of PLA with a corresponding increase in the PLA glass transition located close to the interface. Moreover, the co-continuous morphology of the blend produces a quite large interface extension, with a corresponding non-negligible volume of the polymer located in this region.

Table 2. Thermal transitions by DSC analysis of keratin/PLA blends and PLA with different amounts of GO

Matrix	GO (%)	Tg (°C)	ΔCp (J g^{-1} °C^{-1})	T_1 (°C)	ΔH_1(J g^{-1})
Keratin/PLA	0	56	0.25	96	0.07
	0.1	56	0.27	94	0.19
	0.5	55	0.34	92	0.27
	0.7	56	0.27	94	0.17
	1.0	56	0.30	94	0.08
PLA	0	53	0.51	n.d.	-
	0.5	55	0.58	n.d.	-
	1	55	0.45	n.d.	-

The addition of GO to PLA results in a similar, even if lower by value, shift toward a high temperature of the glass transition observed by mixing with keratin. This suggests a similar effect of GO and keratin on increasing the stiffness of PLA in the interfacial region (Coiai et al., 2013; Prevosto et al., 2010). On the contrary, the addition of GO to the Ker/PLA blend results in Tg values with intermediate values between the ones of pure PLA and Ker/PLA. The observed behavior is similar to the shift of the C=O of PLA observed by FT-IR, for which the ternary mixture exhibits a peak at wavenumber intermediate in-between the values of PLA/GO and Ker/PLA. Therefore, once again the data can be interpreted by the formation of an almost homogenous three components heterophase, namely keratin, PLA domains, and the interface region between them.

Notice that the observed immiscibility by DSC data is in apparent contradiction with the data by rheology. However, this latter refers to the polymers in HFIP solutions, while thermal data refer to the polymer in the solid state. In the case of nanofibers, morphology analysis by SEM and TEM showed a very homogenous phase that is compatible with one of the miscible polymer blends. However, based on thermal information it is more likely that miscibility occurred only under shear in solution. Once HFIP evaporates, the blend components in nanofibers separate. However, for kinetic reasons due to the electrospinning process, we do not see phase separation on the macro-micro scale by microscopy analysis; this could be explained by the formation of nano-sized phase separated domains not detected by microscopy or by the formation of a co-continuous heterophase. This last hypothesis is supported by the rheological behavior that showed either keratin and PLA in the continuous or continuous phase, depending on the GO loading. Additional complexity to the phase arrangement could be induced by the electrical field during electrospinning. In any case, whatever the morphology, due to the formation process, phases are characterized by a lower packing density concerning the bulk phases that usually form under equilibrium conditions. The low packing is in agreement with the blue shift of the PLA adsorption peaks observed by ATR analysis.

The DSC thermograms of keratin/PLA mixtures with GO show, in addition to the glass transition process of PLA, two other processes exhibiting both endothermic peaks (Figure 10a). The broad peak at the highest temperature has a maximum in the 115 – 120 °C range and can be assigned to the residual moisture that was not removed by the first heating treatment up to 105 °C. It is likely due to water bonded to keratin that, as other proteins do, can interact strongly with water shifting its evaporation temperature (Hatakeyama et al., 1988).
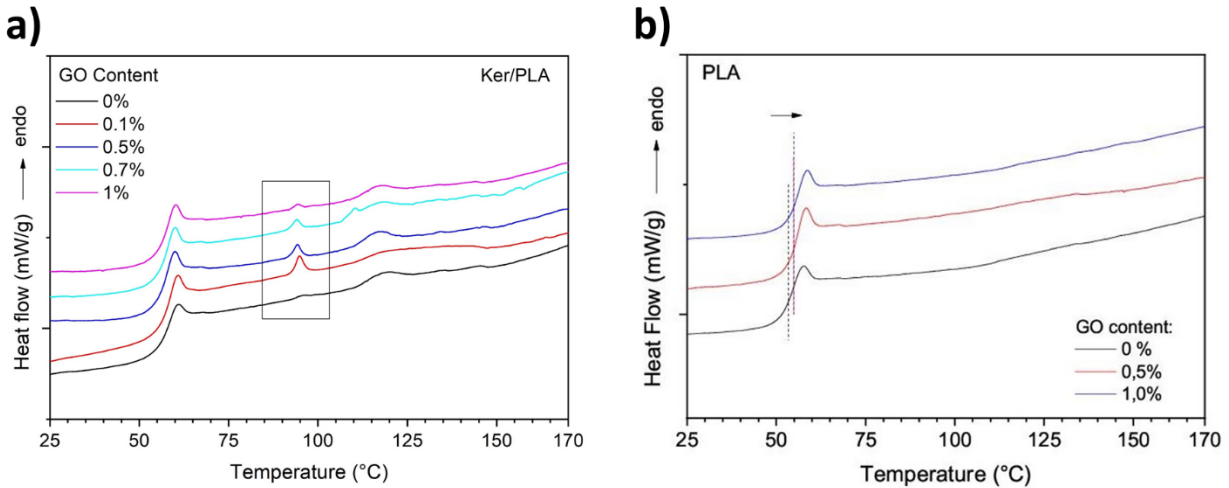
Figure 10. Comparison among DSC thermograms (2° heating step) of keratin/PLA (a) and PLA (b) nanofibers with different amounts of GO. Graphs are arbitrarily vertically shifted for clarity.

The second peak, having maximum, T_1, in the 92-96 °C range (Table 2) was not detected in pure PLA or PLA with GO (Figure 10b) and it is almost not detectable in the Ker/PLA blend. Therefore, it seems to be due to the presence of GO and keratin together. Notice that, to the best of our knowledge a peak at this temperature has never been reported for keratin-based materials. However, materials are often analyzed in a single heating step by DSC (Liu et al., 2018) and this range is covered by the evaporation of unbonded water (Milczarek et al., 1992). Even if this peak is always small in area, it is interesting to observe that the area depends on the GO content: it is very small at 0 % GO, increases with the amount of GO up to 0.5 % of loading, where it is maximum; then, it decreases again and reaches a value close to the one of the net matrix at 1 % loading of GO (Table 2). It is thus evident, that whatever the nature of the peak, the associated process is strongly affected by the presence of GO, the peak being higher when the degree of dispersion of GO is maximum. The analogy between the trend of this peak intensity and viscosity data for increasing GO loading suggests that the endothermic process is correlated to

the different keratin or phases' structural arrangement in the matrix because of the joined GO and flux effects.

3.6 Mechanical Properties. The mechanical properties of nanofibrous mats were evaluated via tensile testing. To discard inaccuracies due to material porosity and thickness measurement, load data were analyzed according to the approach proposed by Maccaferri et al. (Maccaferri et al., 2022; Maccaferri et al., 2020; Maccaferri et al., 2021), by applying the following equation (Eq. 3):

$$\sigma = \rho_m \frac{F}{m} L \tag{3}$$

where σ is the stress (MPa), m is the specimen mass (mg), ρ_m is the material density (mg/mm^3), L is the specimen initial length (mm) and F is the load (N).

Histograms of Figure 11 display mats' tensile properties. GO does not significantly improve the elastic modulus nor strength (maximum stress) of membranes. However, in some cases, reinforced mats have higher mean values, especially when 0.7 % and 1.0 % of GO are loaded (up to +35 % and +23 % in elastic modulus and strength, respectively). By contrast, GO has a stronger impact on strain at break, showing improved deformability as the GO increase. Membranes with 0.5 % and 0.7 % of GO almost double the strain at the break with respect to the unreinforced sample, while adding 1.0 % of GO leads to even better deformation (+135 %). Results display that the addition of GO, regardless of its percentage, does not lower the mechanical properties of Keratin/PLA nanofibrous membranes. Moreover, the sample with the highest GO content shows overall mechanical properties better than the unmodified mat.
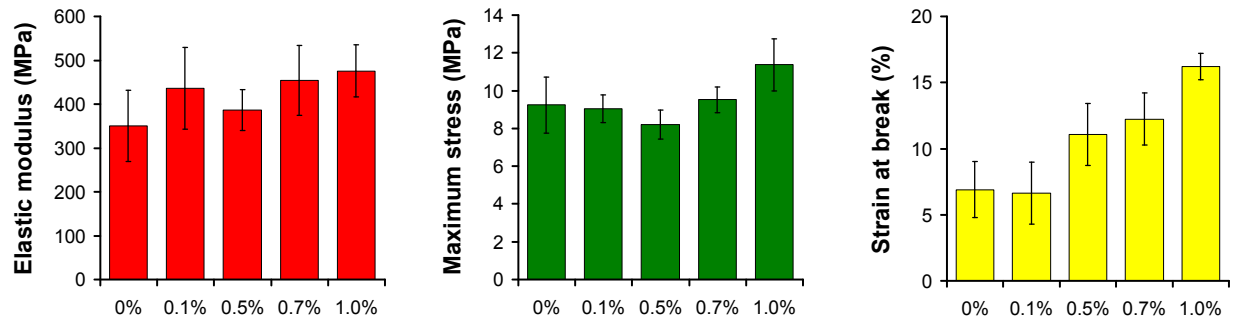
Figure 11. *Elastic modulus, maximum stress and strain at break of keratin/PLA nanofibrous mats as a function of the GO loading.*

3.7 Effect of graphene oxide on drug release. The drug release profiles were determined only on the Ker/PLA mat containing the 0.5 % of GO selected among the GO containing ones, because of its good dispersion of GO sheets, and the Ker/PLA mat without GO as the reference sample. In particular, the aforementioned samples were loaded with a 3 % weight of RhB chosen as a drug model for its easy detectability using UV-Vis measurements (Figure S7).

The profile of cumulative drug release versus time is shown in Figure 12. The release profile of free RhB across the dialysis bag was also determined (as control). As expected, the release of free RhB is very fast reaching a plateau at about 92 % within 2 hours (Figure 12 a) while, in the same time range, the RhB released from the nanofibrous mats is only 10 %. In the final stage of the test (40 h), about 60 % and 40 % of the RhB are released from the mats without and with GO, respectively (Figure 12 b). This indicates that the presence of GO delayed the release of drugs probably because of the strong interactions between RhB and GO sheets by means of hydrogen bonds π-π stacking, and hydrophobic interactions (Zhang et al., 2011).

To better understand the mechanism of drug release, a non-linear data fitting using the Korsmeyer-Peppas model (Eq. 4) was carried out (Korsmeyer et al., 1983):

$$Q_t = kt^n \tag{4}$$

where Q_t (%) is the percentage of the released drug and t (h) is the corresponding time. From the data fitting the transport constants k and the transport exponents n were determined. Considering the nanofibers as cylindric drug delivery systems, an n value of 0.45 indicates Fick diffusion; while, higher values between 0.45 and 0.89 indicates anomalous transport involving both Fickian diffusion and matrix swelling contribution (Costa and Sousa Lobo, 2001). The two samples have the same k value (Table 3), therefore it seems that the GO does not modify the diffusion rate of the drug. However, the n value for the mat without GO falls in the 0.45-0.89 range, indicating an anomalous transport; on the contrary, the mat with the GO showed a value of n of 0.45, indicating a pure Fickian diffusion of the drug.

In order to evaluate the dependence degree of the drug release upon the Fickian diffusion and matrix swelling contribution, the Peppas-Salhin model (Peppas and Sahlin, 1989), described in Eq. 5 was applied:

$$Q_t = k_d t^{0.45} + k_r t^{0.90} \tag{5}$$

where k_d represents the Fickian diffusional contribution, while k_r is the matrix swelling one (Di Prima et al., 2020). The values obtained for k_r by a best fitting procedure of the release data are comparable for the samples with and without GO. Furthermore, the values are more or less the same as the ones obtained by fitting with eq (4). On the contrary, the relaxational contribution of matrix swelling, k_d is zero for the mat with GO, while, even though small it is present for the matrix without GO. Therefore, even if the drug is released mainly by a Fickian diffusion mechanism in both investigated samples, in the absence of GO a minor contribution due to the matrix swelling is present. This behavior supports the hypothesis that the GO reduces the swellability of the keratin rich domains resulting in a Fickian controlled diffusion of the model drug in the composite nanofiber mat.
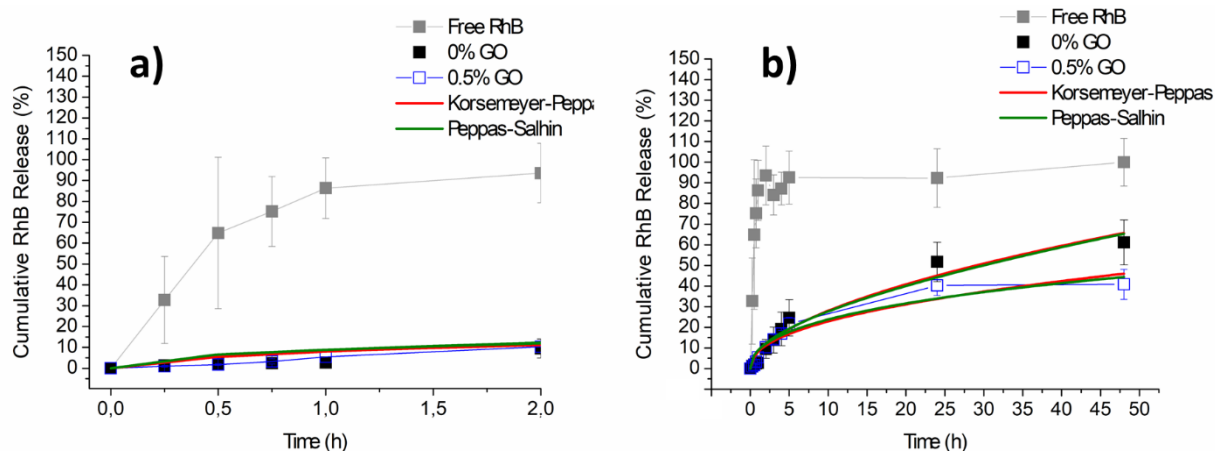
Figure 12. *The RhB release profiles and mathematical curve fitting by Korsemeyer-Peppas and Peppas-Salhin models. Detail of the first 2 hours' release (a) and complete release profile (b)*

Table 3. *Kinetic parameters of RhB released from the keratin/PLA 50/50 electrospun mats with 0.5 % of GO and without GO*

GO (%)	Korsemeyer-Peppas			Peppas-Salhin		
	k (h^{-n})	n	R^2	k_d(h$^{-0.45}$)	k_r(h$^{-0.45}$)	R^2
0	8±1	0.54±0.05	0.957	8±1	0.6±0.4	0.948
0.5	8±1	0.44±0.05	0.924	9±1	*-0.2±0.3*	0.929

CONCLUSION

In summary, an innovative electrospun mat made of an unprecedented ternary composite system constituted by a keratin/PLA blend matrix filled with GO sheets was here developed for controlled drug delivery applications. In particular, keratin has been selected as an interesting non-food protein for the design of drug delivery systems due to its biocompatibility, bioactivity, and biodegradability. An additional advantage of keratin is its production from byproducts of the dairy and slaughterhouse industries. On the other hand, PLA is a valid support polymer with an acceptable biodegradability and good biocompatibility that significantly improve the processing of keratin by electrospinning. Finally, GO sheets were selected as filler to improve both the rheological characteristics of the polymer blend solution, as well as to better control the drug

release kinetics. A series of Ker/PLA 50/50 mats loaded with different amounts of GO were here prepared by electrospinning at different applied voltages. As expected, the GO added to the solvent contributed to increasing its conductivity. Moreover, a GO loading from 0.1 to 0.5 % contributes to increasing the viscosities and the yield-stress behavior of Ker/PLA 50/50 blend solutions. At higher GO loading, a different phase blends morphology builds up with PLA in the continuous phase a more moderate effect of the GO incorporation on the solution viscosity.

The nanofibers' diameter depended on both the applied voltage and on the GO loading in a complex manner. Indeed, GO addition increases both the viscosity and the conductivity of the solution, the former resulting in thicker fibers while the latter promote thinner ones. Furthermore, the higher applied voltage increase the polarization and the deposition rate. As result at lower applied voltages of 12 and 15 kV (lower applied stretching) the nanofibers thinning is affected by the conductivity as well as by the shear thinning behavior of the starting dispersion. In this condition, the relatively high conductivity and the pronounced shear thinning resulting from the loading of 0.5 % of GO seems to promote the formation of the thinnest nanofibers. Instead, at the high applied voltage, the dominant effect is the one of the viscosity, which increases with the GO loading. Under this condition, the thinnest and most homogeneous nanofibers were obtained at all investigated GO contents. The GO sheets were embedded into the nanofibers and some of them form protruding bulges. Nevertheless, this does not compromise the mechanical properties of the final mats; rather, a GO loading of 1 % contributes to improving the maximum stress and the strain at break. Moreover, also the thermal stability and the degradation pathway of the electrospun mats are not affected by the presence of GO.

At the macromolecular level, some weak interfacial interactions involving the carbonyl groups of the two polymers, occur between keratin and PLA as well as on GO and PLA interfacial regions as revealed by ATR analysis. The GO sheets presumably do not interfere with the keratin secondary structures; nevertheless, higher-level rearrangements of the protein chains seem to be affected by a joined action of low GO loadings and flux conditions. Finally, the main effect of GO on the drug release is to reduce the swelling of the matrix, thereby slowing down RhB release from the mats.

The obtained results demonstrate the potential of Ker/PLA/GO electrospun mats for applications in drug delivery. In particular, the knowledge of the effect of GO on the electrospinning process and chemical-physical properties of Ker/PLA mats, as well as on the drug release here acquired

is fundamental for the design of patches that display desired mechanical properties and desired kinetics and mechanisms of drug release, to be obtained by additive electrospinning of different nanofibrous layers. The main advantage of such knowledge lies in the possibility to have a ternary system with combined and modularly properties in terms of electrospinability, nanometric morphology, and mechanical and drug release properties.

GRAPHICAL ABSTRACT
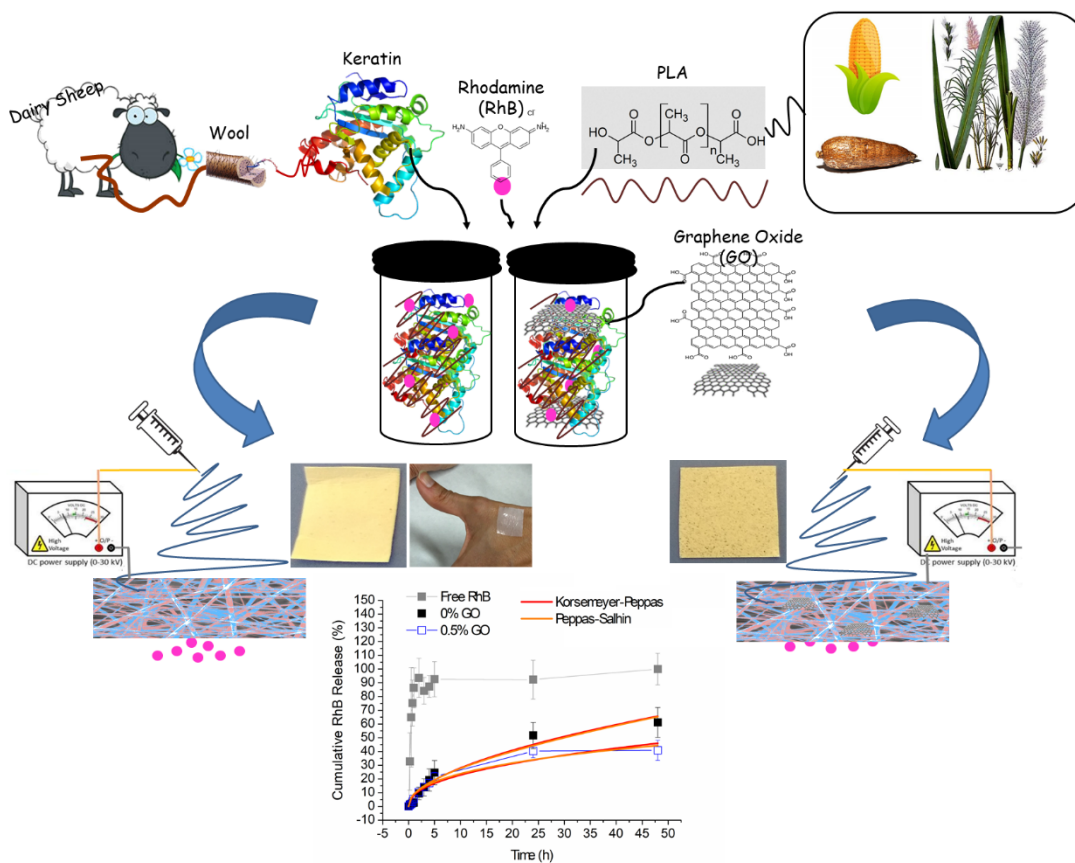
ASSOCIATED CONTENT – Video about the application of the electrospun mats (without GO and/or RhB), on the wet skin.

Supporting Information. Shear viscosity (η) of the GO in hexafluoroisopropanol (HFIP) at different concentrations; Diameters distribution of electrospun fibers from Ker/PLA 50/50 solutions with different loadings of GO sheets fitted with the LogNormal function; Conductivity of the solutions of GO dispersed in 1,1,1,3,3,3 hexafluoroisopropanol as function of GO amount; Selected Area Electron Diffraction images of the Keratin/PLA/GO composite on left) bulging nanosheet and right) pristine nanofiber. The reference HR-TEM micrograph in the inset displays the relative position of each diffraction image. The diffractogram on the bulging GO nanosheet displays sharper diffraction rings at 2.1 and 4.0 Å relative to semi-crystalline GO; Comparison between the TGA plots of PLA and PLA/GO 0.5 % carried out under nitrogen atmosphere; electrospun mat made of keratin/PLA 50/50 and 0.5 % of GO, loaded with 3 % of Rhodamine B (RhB).

Corresponding Authors:

Annalisa Aluigi, Department of Biomolecular Sciences - School of Pharmacy, University of Urbino, Piazza del Rinascimento 6 - 61029 Urbino, Italy – email: Annalisa.aluigi@uniurb.it

Monica Bertoldo, Department of Industrial Chemistry "Toso Montanari", University of Bologna, Viale Risorgimento 4, 40126 Bologna, Italy – email: brtmnc@unife.it

Author Contributions

The manuscript was written with contributions of all authors. All authors have approved the final version of the manuscript.

REFERENCES

Akhmetova, A., Heinz, A., 2020. Electrospinning Proteins for Wound Healing Purposes: Opportunities and Challenges. Pharmaceutics 13, 4. https://doi.org/10.3390/pharmaceutics13010004

Aluigi, A., Sotgiu, G., Torreggiani, A., Guerrini, A., Orlandi, V.T., Corticelli, F., Varchi, G., 2015. Methylene Blue Doped Films of Wool Keratin with Antimicrobial Photodynamic Activity. ACS Appl. Mater. Interfaces 7, 17416–17424. https://doi.org/10.1021/acsami.5b04699

Beliciu, C.M., Moraru, C.I., 2011. The effect of protein concentration and heat treatment temperature on micellar casein–soy protein mixtures. Food Hydrocoll. 25, 1448–1460. https://doi.org/10.1016/j.foodhyd.2011.01.011

Castellanos, M.M., Pathak, J.A., Colby, R.H., 2014. Both protein adsorption and aggregation contribute to shear yielding and viscosity increase in protein solutions. Soft Matter 10, 122–131. https://doi.org/10.1039/C3SM51994E

Choi, H.J., Kim, S.G., Hyun, Y.H., Jhon, M.S., 2001. Preparation and Rheological Characteristics of Solvent-Cast Poly(ethylene oxide)/Montmorillonite Nanocomposites. Macromol. Rapid Commun. 22, 320–325. https://doi.org/10.1002/1521-3927(20010301)22:5<320::AID-MARC320>3.0.CO;2-3

Chopra, D., Haynes, C., Hatzikiriakos, S.G., Vlassopoulos, D., 1999. Modeling the shear-induced structural changes in polymeric fluids. J. Nonnewton. Fluid Mech. 82, 367–385. https://doi.org/10.1016/S0377-0257(98)00172-4

Coiai, S., Prevosto, D., Bertoldo, M., Conzatti, L., Causin, V., Pinzino, C., Passaglia, E., 2013. Chemistry of Interfacial Interactions in a LDPE-Based Nanocomposite and Their Effect on the Nanoscale Hybrid Assembling. Macromolecules 46, 1563–1572. https://doi.org/10.1021/ma301689h

Costa, P., Sousa Lobo, J.M., 2001. Modeling and comparison of dissolution profiles. Eur. J. Pharm. Sci. 13, 123–133. https://doi.org/10.1016/S0928-0987(01)00095-1

Croitoru, A.-M., Karaçelebi, Y., Saatcioglu, E., Altan, E., Ulag, S., Aydoğan, H.K., Sahin, A., Motelica, L., Oprea, O., Tihauan, B.-M., Popescu, R.-C., Savu, D., Trusca, R., Ficai, D., Gunduz, O., Ficai, A., 2021. Electrically Triggered Drug Delivery from Novel Electrospun

Poly(Lactic Acid)/Graphene Oxide/Quercetin Fibrous Scaffolds for Wound Dressing Applications. Pharmaceutics 13, 957. https://doi.org/10.3390/pharmaceutics13070957

Datta, L.P., Manchineella, S., Govindaraju, T., 2020. Biomolecules-derived biomaterials. Biomaterials 230, 119633. https://doi.org/10.1016/j.biomaterials.2019.119633

Dhivya, S., Padma, V.V., Santhini, E., 2015. Wound dressings – a review. BioMedicine 5, 22. https://doi.org/10.7603/s40681-015-0022-9

Di Prima, G., Campisi, G., De Caro, V., 2020. Amorphous Ropinirole-Loaded Mucoadhesive Buccal Film: A Potential Patient-Friendly Tool to Improve Drug Pharmacokinetic Profile and Effectiveness. J. Pers. Med. 10, 242. https://doi.org/10.3390/jpm10040242

Eren Boncu, T., Ozdemir, N., Uskudar Guclu, A., 2020. Electrospinning of linezolid loaded PLGA nanofibers: effect of solvents on its spinnability, drug delivery, mechanical properties, and antibacterial activities. Drug Dev. Ind. Pharm. 46, 109–121. https://doi.org/10.1080/03639045.2019.1706550

Esparza, Y., Ullah, A., Wu, J., 2017. Preparation and characterization of graphite oxide nano-reinforced biocomposites from chicken feather keratin. J. Chem. Technol. Biotechnol. 92, 2023–2031. https://doi.org/10.1002/jctb.5196

García-Abuín, A., Gómez-Díaz, D., Navaza, J.M., Quintáns-Riveiro, L.C., 2010. Viscosimetric behaviour of carboxymethyl cellulose – Arabic gum mixtures: A new step to modelling. Carbohydr. Polym. 80, 26–30. https://doi.org/10.1016/j.carbpol.2009.10.064

Gasparini, C., Aluigi, A., Pace, G., Molina-García, M.A., Treossi, E., Ruani, G., Candini, A., Melucci, M., Bettin, C., Bonaccorso, F., Liscio, A., Palermo, V., 2020. Enhancing triboelectric performances of electrospun poly(vinylidene fluoride) with graphene oxide sheets. Graphene Technol. 5, 49–57. https://doi.org/10.1007/s41127-020-00038-w

Giuri, D., Barbalinardo, M., Sotgiu, G., Zamboni, R., Nocchetti, M., Donnadio, A., Corticelli, F., Valle, F., Gennari, C.G.M., Selmin, F., Posati, T., Aluigi, A., 2019. Nano-hybrid electrospun non-woven mats made of wool keratin and hydrotalcites as potential bio-active wound dressings. Nanoscale 11, 6422–6430. https://doi.org/10.1039/C8NR10114K

Guidotti, G., Soccio, M., Bondi, E., Posati, T., Sotgiu, G., Zamboni, R., Torreggiani, A., Corticelli, F., Lotti, N., Aluigi, A., 2021. Effects of the Blending Ratio on the Design of Keratin/Poly(butylene succinate) Nanofibers for Drug Delivery Applications. Biomolecules 11, 1194. https://doi.org/10.3390/biom11081194

Haider, A., Haider, S., Kang, I.-K., 2018. A comprehensive review summarizing the effect of electrospinning parameters and potential applications of nanofibers in biomedical and biotechnology. Arab. J. Chem. 11, 1165–1188. https://doi.org/10.1016/j.arabjc.2015.11.015

Hatakeyama, T., Nakamura, K., Hatakeyama, H., 1988. Determination of bound water content in polymers by DTA, DSC and TG. Thermochim. Acta 123, 153–161. https://doi.org/10.1016/0040-6031(88)80018-2

Hauswirth, S.C., Bowers, C.A., Fowler, C.P., Schultz, P.B., Hauswirth, A.D., Weigand, T., Miller, C.T., 2020. Modeling cross model non-Newtonian fluid flow in porous media. J. Contam. Hydrol. 235, 103708. https://doi.org/10.1016/j.jconhyd.2020.103708

Heikkila, P., Harlin, A., 2009. Electrospinning of polyacrylonitrile (PAN) solution: Effect of conductive additive and filler on the process. Express Polym. Lett. 3, 437–445. https://doi.org/10.3144/expresspolymlett.2009.53

Horst, R., Wolf, B.A., 1997. Phase diagrams calculated for sheared ternary polymer blends. Polymer (Guildf). 38, 4697–4703. https://doi.org/10.1016/S0032-3861(96)01076-2

Hyun, Y.H., Lim, S.T., Choi, H.J., Jhon, M.S., 2001. Rheology of Poly(ethylene oxide)/Organoclay Nanocomposites. Macromolecules 34, 8084–8093. https://doi.org/10.1021/ma002191w

Isarankura Na Ayutthaya, S., Tanpichai, S., Sangkhun, W., Wootthikanokkhan, J., 2016. Effect of clay content on morphology and processability of electrospun keratin/poly(lactic acid) nanofiber. Int. J. Biol. Macromol. 85, 585–595. https://doi.org/10.1016/j.ijbiomac.2016.01.041

Jabarin, S.A., Majdzadeh-Ardakani, K., Lofgren, E.A., 2016. Crystallization and Melting Behavior in Polymer Blends, in: Encyclopedia of Polymer Blends. Wiley-VCH Verlag GmbH & Co. KGaA, Weinheim, Germany, pp. 135–190. https://doi.org/10.1002/9783527653966.ch2

Jupp, L., Kawakatsu, T., Yuan, X.-F., 2003. Modeling shear-induced phase transitions of binary polymer mixtures. J. Chem. Phys. 119, 6361–6372. https://doi.org/10.1063/1.1601214

Korsmeyer, R.W., Gurny, R., Doelker, E., Buri, P., Peppas, N.A., 1983. Mechanisms of solute release from porous hydrophilic polymers. Int. J. Pharm. 15, 25–35. https://doi.org/10.1016/0378-5173(83)90064-9

Krysiak, Z.J., Knapczyk-Korczak, J., Maniak, G., Stachewicz, U., 2021. Moisturizing effect of

skin patches with hydrophobic and hydrophilic electrospun fibers for atopic dermatitis. Colloids Surfaces B Biointerfaces 199, 111554. https://doi.org/10.1016/j.colsurfb.2020.111554

Li, J., Li, Y., Li, L., Mak, A.F.T., Ko, F., Qin, L., 2009. Preparation and biodegradation of electrospun PLLA/keratin nonwoven fibrous membrane. Polym. Degrad. Stab. 94, 1800–1807. https://doi.org/10.1016/j.polymdegradstab.2009.06.004

Li, Z., Wang, R., Wu, S., Xue, Z., Zhu, D., Zou, J., Li, X., 2021. In situ observation of metal ion interactions with graphene oxide layers: From the growth of metal hydroxide to metal oxide formation. Carbon N. Y. 184, 721–727. https://doi.org/10.1016/j.carbon.2021.08.073

Liu, C., Shen, J., Yeung, K.W.K., Tjong, S.C., 2017. Development and Antibacterial Performance of Novel Polylactic Acid-Graphene Oxide-Silver Nanoparticle Hybrid Nanocomposite Mats Prepared By Electrospinning. ACS Biomater. Sci. Eng. 3, 471–486. https://doi.org/10.1021/acsbiomaterials.6b00766

Liu, R., Li, L., Liu, S., Li, S., Zhu, X., Yi, M., Liao, X., 2018. Structure and properties of wool keratin/poly (vinyl alcohol) blended fiber. Adv. Polym. Technol. 37, 2756–2762. https://doi.org/10.1002/adv.21948

Luraghi, A., Peri, F., Moroni, L., 2021. Electrospinning for drug delivery applications: A review. J. Control. Release 334, 463–484. https://doi.org/10.1016/j.jconrel.2021.03.033

Maccaferri, E., Cocchi, D., Mazzocchetti, L., Benelli, T., Brugo, T.M., Giorgini, L., Zucchelli, A., 2021. How Nanofibers Carry the Load: Toward a Universal and Reliable Approach for Tensile Testing of Polymeric Nanofibrous Membranes. Macromol. Mater. Eng. 306, 2100183. https://doi.org/10.1002/mame.202100183

Maccaferri, E., Mazzocchetti, L., Benelli, T., Brugo, T.M., Zucchelli, A., Giorgini, L., 2022. Self-Assembled NBR/Nomex Nanofibers as Lightweight Rubbery Nonwovens for Hindering Delamination in Epoxy CFRPs. ACS Appl. Mater. Interfaces 14, 1885–1899. https://doi.org/10.1021/acsami.1c17643

Maccaferri, E., Mazzocchetti, L., Benelli, T., Brugo, T.M., Zucchelli, A., Giorgini, L., 2020. Rubbery nanofibers by co-electrospinning of almost immiscible NBR and PCL blends. Mater. Des. 186, 108210. https://doi.org/10.1016/j.matdes.2019.108210

Mao, Z., Li, J., Huang, W., Jiang, H., Zimba, B.L., Chen, L., Wan, J., Wu, Q., 2018. Preparation of poly(lactic acid)/graphene oxide nanofiber membranes with different structures by

electrospinning for drug delivery. RSC Adv. 8, 16619–16625. https://doi.org/10.1039/C8RA01565A

Milczarek, P., Zielinski, M., Garcia, M.L., 1992. The mechanism and stability of thermal transitions in hair keratin. Colloid Polym. Sci. 270, 1106–1115. https://doi.org/10.1007/BF00652875

Na Ayutthaya, S.I., Woothikanokkhan, J., 2013. Extraction of Keratin from Chicken Feather and Electrospinning of the Keratin/PLA Blends. Adv. Mater. Res. 747, 711–714. https://doi.org/10.4028/www.scientific.net/AMR.747.711

Otsuki, A., 2020. Rheology of colloidal particle suspensions, in: Rheology of Polymer Blends and Nanocomposites. Elsevier, pp. 49–71. https://doi.org/10.1016/B978-0-12-816957-5.00004-5

Pakravan, M., Heuzey, M.-C., Ajji, A., 2012. Determination of Phase Behavior of Poly(ethylene oxide) and Chitosan Solution Blends Using Rheometry. Macromolecules 45, 7621–7633. https://doi.org/10.1021/ma301193h

Peppas, N.A., Sahlin, J.J., 1989. A simple equation for the description of solute release. III. Coupling of diffusion and relaxation. Int. J. Pharm. 57, 169–172. https://doi.org/10.1016/0378-5173(89)90306-2

Posati, T., Giuri, D., Nocchetti, M., Sagnella, A., Gariboldi, M., Ferroni, C., Sotgiu, G., Varchi, G., Zamboni, R., Aluigi, A., 2018. Keratin-hydrotalcites hybrid films for drug delivery applications. Eur. Polym. J. 105, 177–185. https://doi.org/10.1016/j.eurpolymj.2018.05.030

Prevosto, D., Lucchesi, M., Bertoldo, M., Passaglia, E., Ciardelli, F., Rolla, P., 2010. Interfacial effects on the dynamics of ethylene–propylene copolymer nanocomposite with inorganic clays. J. Non. Cryst. Solids 356, 568–573. https://doi.org/10.1016/j.jnoncrysol.2009.09.035

Ramazani, S., Karimi, M., 2015. Aligned poly(ε-caprolactone)/graphene oxide and reduced graphene oxide nanocomposite nanofibers: Morphological, mechanical and structural properties. Mater. Sci. Eng. C 56, 325–334. https://doi.org/10.1016/j.msec.2015.06.045

Rostami, F., Tamjid, E., Behmanesh, M., 2020. Drug-eluting PCL/graphene oxide nanocomposite scaffolds for enhanced osteogenic differentiation of mesenchymal stem cells. Mater. Sci. Eng. C 115, 111102. https://doi.org/10.1016/j.msec.2020.111102

Sabet, M., Soleimani, H., Mohammadian, E., Hosseini, S., 2020. Impact of inclusion of graphene oxide nanosheets on polypropylene thermal characteristics. Iran. Polym. J. 29, 1099–1112.

https://doi.org/10.1007/s13726-020-00864-y

Sadeghi, S., Nourmohammadi, J., Ghaee, A., Soleimani, N., 2020. Carboxymethyl cellulose-human hair keratin hydrogel with controlled clindamycin release as antibacterial wound dressing. Int. J. Biol. Macromol. 147, 1239–1247. https://doi.org/10.1016/j.ijbiomac.2019.09.251

Saini, P., Arora, M., Kumar, M.N.V.R., 2016. Poly(lactic acid) blends in biomedical applications. Adv. Drug Deliv. Rev. 107, 47–59. https://doi.org/10.1016/j.addr.2016.06.014

Samadi, S., Moradkhani, M., Beheshti, H., Irani, M., Aliabadi, M., 2018. Fabrication of chitosan/poly(lactic acid)/graphene oxide/TiO2 composite nanofibrous scaffolds for sustained delivery of doxorubicin and treatment of lung cancer. Int. J. Biol. Macromol. 110, 416–424. https://doi.org/10.1016/j.ijbiomac.2017.08.048

Sharma, V., Jaishankar, A., Wang, Y.-C., McKinley, G.H., 2011. Rheology of globular proteins: apparent yield stress, high shear rate viscosity and interfacial viscoelasticity of bovine serum albumin solutions. Soft Matter 7, 5150. https://doi.org/10.1039/c0sm01312a

Tan, Y., Song, Y., Zheng, Q., 2012. Hydrogen bonding-driven rheological modulation of chemically reduced graphene oxide/poly(vinyl alcohol) suspensions and its application in electrospinning. Nanoscale 4, 6997. https://doi.org/10.1039/c2nr32160b

Teodorescu, M., Bercea, M., Morariu, S., 2018. Miscibility study on polymer mixtures in dilute solution. Colloids Surfaces A Physicochem. Eng. Asp. 559, 325–333. https://doi.org/10.1016/j.colsurfa.2018.09.062

Tonin, C., Aluigi, A., Varesano, A., Vineis, C., 2010. Keratin-based Nanofibres, in: Nanofibers. InTech. https://doi.org/10.5772/8151

Ulker Turan, C., Guvenilir, Y., 2021. Fabrication and characterization of electrospun biopolyester/gelatin nanofibers. J. Biomed. Mater. Res. Part B Appl. Biomater. 109, 1478–1487. https://doi.org/10.1002/jbm.b.34807

Verma, V., Verma, P., Ray, P., Ray, A.R., 2008. Preparation of scaffolds from human hair proteins for tissue-engineering applications. Biomed. Mater. 3, 025007. https://doi.org/10.1088/1748-6041/3/2/025007

Wu, S., Chen, X., Li, T., Cui, Y., Yi, M., Ge, J., Yin, G., Li, X., He, M., 2020. Improving the Performance of Feather Keratin/Polyvinyl Alcohol/Tris(hydroxymethyl)Aminomethane Nanocomposite Films by Incorporating Graphene Oxide or Graphene. Nanomaterials 10,

327. https://doi.org/10.3390/nano10020327

Xiao, J., Tan, Y., Song, Y., Zheng, Q., 2016. Simultaneous regulation of morphology, crystallization, thermal stability and adsorbability of electrospun polyamide 6 nanofibers via graphene oxide and chemically reduced graphene oxide. RSC Adv. 6, 41392–41403. https://doi.org/10.1039/C6RA05255J

Yang, C., Yan, Z., Lian, Y., Wang, J., Zhang, K., 2020. Graphene oxide coated shell-core structured chitosan/PLLA nanofibrous scaffolds for wound dressing. J. Biomater. Sci. Polym. Ed. 31, 622–641. https://doi.org/10.1080/09205063.2019.1706149

Yassin, A.Y., Abdelghany, A.M., 2021. Synthesis and thermal stability, electrical conductivity and dielectric spectroscopic studies of poly (ethylene-co-vinyl alcohol)/graphene oxide nanocomposite. Phys. B Condens. Matter 608, 412730. https://doi.org/10.1016/j.physb.2020.412730

Zhang, J., Tsuji, H., Noda, I., Ozaki, Y., 2004. Structural Changes and Crystallization Dynamics of Poly(l-lactide) during the Cold-Crystallization Process Investigated by Infrared and Two-Dimensional Infrared Correlation Spectroscopy. Macromolecules 37, 6433–6439. https://doi.org/10.1021/ma049288t

Zhang, M., Ding, X., Zhan, Y., Wang, Y., Wang, X., 2020. Improving the flame retardancy of poly(lactic acid) using an efficient ternary hybrid flame retardant by dual modification of graphene oxide with phenylphosphinic acid and nano MOFs. J. Hazard. Mater. 384, 121260. https://doi.org/10.1016/j.jhazmat.2019.121260

Zhang, R., Hummelgård, M., Lv, G., Olin, H., 2011. Real time monitoring of the drug release of rhodamine B on graphene oxide. Carbon N. Y. 49, 1126–1132. https://doi.org/10.1016/j.carbon.2010.11.026

Zhou, T., Zhou, X., Xing, D., 2014. Controlled release of doxorubicin from graphene oxide based charge-reversal nanocarrier. Biomaterials 35, 4185–4194. https://doi.org/10.1016/j.biomaterials.2014.01.044

Author Contributions:

Annalisa Aluigi: She worked on the conceptualization of the work. As supervisor of Gioacchino Schifino (Ph.D.student) and Simon Drudi (Master Degree Student), she coordinated all the work, from the data collection and discussion to the drafting of the manuscript. He particularly coordinated the electrospinning and drug release activities. She dealt with the original draft writing and editing as well as with the review of the final draft. As a member of Kerline, she also contributed in the characterization of keratin powder produced within Kerline.

Monica Bertoldo: She collaborated on conceptualization draft writing and review of the work. She particularly contributed to the data analysis and discussion related to the rheological and thermal behavior of the samples.

Gioacchino Schifino (Ph.D. student): Under the supervision of Annalisa Aluigi, he worked on the preparation of samples by electrospinning and the collection of rheological data of the electrospinning solutions.

Claudio Gasparini (Ph.D. student)**:** Under the supervision of Emanuele Treossi and Monica Bertoldo, he worked on the characterization of GO sheets and the collection and discussion of the DSC and TGA thermograms.

Simone Drudi (Master degree student)**:** Under the supervision of Annalisa Aluigi, he dealt with the collection of the drug release data. He contributed to the discussion about the drug release mechanism and kinetics.

Marta Giannelli (Ph.D. student)**:** Under the supervision of Tamara Posati, she was involved in the collection and discussion of the FTIR-ATR data.

Giovanna Sotgiu: She was involved in the collection of SEM images and discussion of morphological data. As a member of Kerline, she also contributed to the production of keratin powder

Tamara Posati: As scientific supervisor of Marta Giannelli, she coordinated the activities related to the collection and discussion of FTIR analysis.

Roberto Zamboni: As the group leader, he contributed to the discussion of the FTIR-ATR data. As a member of Kerline, he also contributed to the production of keratin powder.

Emanuele Treossi: As supervisor of Claudio Gasparini, he contributed to the characterization of GO sheets.

Emanuele Maccaferri: Under the supervision of Loris Giorgini, he worked on the collection and discussion of the mechanical data.

Loris Giorgini: As supervisor of Emanuele Maccaferri, he coordinated the activities related to the mechanical characterizations and relative discussion of the data.

Raffaello Mazzarro: He worked on the collection and discussion of the TEM analysis

Vittorio Morandi: As supervisor of Raffaello Mazzarro, he coordinated the activities related to the TEM characterizations and relative discussion of the data.

Vincenzo Palermo: As the leader of the graphene group he contributed to the revision of the work.